The CDX1–microRNA-215 axis regulates colorectal cancer stem cell differentiation

Matthew F. Jones[a,b], Toshifumi Hara[b], Princy Francis[c], Xiao Ling Li[b], Sven Bilke[c], Yuelin Zhu[c], Marbin Pineda[c], Murugan Subramanian[b], Walter F. Bodmer[a,1], and Ashish Lal[b,1]

[a]Cancer and Immunogenetics Laboratory, Weatherall Institute of Molecular Medicine, Department of Oncology, University of Oxford, John Radcliffe Hospital, Oxford, OX3 9DS, United Kingdom; and [b]Regulatory RNAs and Cancer Section and [c]Molecular Genetics Section, Genetics Branch, Center for Cancer Research, National Cancer Institute, National Institutes of Health, Bethesda, MD 20892

Contributed by Walter F. Bodmer, February 22, 2015 (sent for review December 17, 2014; reviewed by Calvin Kuo and Nicholas A. Wright)

The transcription factor caudal-type homeobox 1 (CDX1) is a key regulator of differentiation in the normal colon and in colorectal cancer (CRC). CDX1 activates the expression of enterocyte genes, but it is not clear how the concomitant silencing of stem cell genes is achieved. MicroRNAs (miRNAs) are important mediators of gene repression and have been implicated in tumor suppression and carcinogenesis, but the roles of miRNAs in differentiation, particularly in CRC, remain poorly understood. Here, we identified microRNA-215 (miR-215) as a direct transcriptional target of CDX1 by using high-throughput small RNA sequencing to profile miRNA expression in two pairs of CRC cell lines: CDX1-low HCT116 and HCT116 with stable CDX1 overexpression, and CDX1-high LS174T and LS174T with stable CDX1 knockdown. Validation of candidate miRNAs identified by RNA-seq in a larger cell-line panel revealed miR-215 to be most significantly correlated with CDX1 expression. Quantitative ChIP–PCR and promoter luciferase assays confirmed that CDX1 directly activates miR-215 transcription. miR-215 expression is depleted in FACS-enriched cancer stem cells compared with unsorted samples. Overexpression of miR-215 in poorly differentiated cell lines causes a decrease in clonogenicity, whereas miR-215 knockdown increases clonogenicity and impairs differentiation in CDX1-high cell lines. We identified the genome-wide targets of miR-215 and found that miR-215 mediates the repression of cell cycle and stemness genes downstream of CDX1. In particular, the miR-215 target gene BMI1 has been shown to promote stemness and self-renewal and to vary inversely with CDX1. Our work situates miR-215 as a link between CDX1 expression and BMI1 repression that governs differentiation in CRC.

miRNA | miR-215 | CDX1 | cancer stem cells | colorectal cancer

The caudal-type homeobox 1 (CDX1) transcription factor controls enterocyte differentiation in the colon, where its expression is excluded from the crypt-base stem cell compartment. CDX1 is also central to the capacity of a colorectal cancer (CRC) cell line to differentiate, and it is a negative marker of CRC stem cells (1–3). In 19% of CRC cell lines assayed in a large study, CDX1 expression was completely lost due to promoter methylation and was down-regulated in a further 13% as a result of hemimethylation of the promoter (4). Comparison of CDX1 expression in colorectal adenocarcinoma versus matched normal tissue showed down-regulation of CDX1 in 73% of tumors, which was also attributable to promoter methylation (5). Expression of CDX1 also correlates inversely with that of the polycomb complex protein BMI1, which is necessary for the maintenance of quiescent injury-inducible stem cells in the normal crypt and is expressed in cancer stem cells (2, 6–8). The mechanism underlying this inverse correlation has not yet been elucidated.

In addition to these correlative data, CDX1 has also been shown to promote directly the expression of structural proteins important for epithelial differentiation including cytokeratin 20 (KRT20) (1), villin (VIL) (9), and FABP1 (10). Introduction of CDX1 into poorly differentiated, non–lumen-forming cell lines that do not express endogenous CDX1 induces lumen formation in three-dimensional (3D) cell culture (2). Transgenic expression of *Cdx1* in mouse gastric epithelium causes intestinal transdifferentiation (11, 12), which supports the observation that CDX1 is up-regulated in Barrett's metaplasia of the esophagus (13). Although several transcriptional targets and functional effects of CDX1 have been identified, there remains much to learn about the mechanisms by which it promotes differentiation and, in particular, those by which it inhibits stemness.

MicroRNAs (miRNAs) are an abundant class of small, 18–22-nt gene regulatory RNAs that have been shown, over the past decade, to be intimately involved in both normal physiological function and disease pathology (14, 15). Many cancers exhibit a global down-regulation of miRNA expression (16, 17), often mediated by underexpression of Dicer or other genes involved in miRNA biogenesis (18). MiRNAs are also frequently located near fragile sites in the genome, as well as commonly amplified regions or common breakpoints, indicating that genomic instability can also result in miRNA dysregulation (19). Aberrant expression or mutation of transcription factors may also result in dysregulation of miRNA expression in cancer, a phenomenon that has been extensively studied in relation to p53 (20–24). However, there is little information regarding the miRNAs regulated by CDX1 and how miRNAs contribute to the effects of CDX1 on stem cells and differentiation in CRC. Here we use small RNA sequencing to identify miRNAs regulated by CDX1. We characterize microRNA-215 (miR-215) as an effector of

Significance

In the colon, stem cell self-renewal and multipotency is regulated by the polycomb complex protein BMI1, among other genes. Differentiation is regulated by the transcription factor caudal-type homeobox 1 (CDX1), expression of which coincides with repression of BMI1. Colorectal cancer stem cells (CSCs) express BMI1 but not CDX1. Tumors that silence CDX1 have a higher proportion of CSCs and an undifferentiated histology, whereas aberrant CDX1 expression is associated with intestinal metaplasias such as Barrett's esophagus. We have identified microRNA-215 (miR-215) as a target of CDX1 in colon cancer that mediates repression of BMI1. MiR-215 operates downstream of CDX1 to promote differentiation and inhibit stemness. In combination with recent advances in the therapeutic uses of small RNAs, miR-215 could offer a novel method to specifically target CSCs.

Author contributions: M.F.J., W.F.B., and A.L. designed research; M.F.J., T.H., P.F., X.L.L., and M.P. performed research; M.F.J., S.B., Y.Z., M.S., W.F.B., and A.L. analyzed data; and M.F.J., W.F.B., and A.L. wrote the paper.

Reviewers: C.K., Stanford University; and N.A.W., Barts and the London School of Medicine.

The authors declare no conflict of interest.

[1]To whom correspondence may be addressed. Email: walter.bodmer@hertford.ox.ac.uk or ashish.lal@nih.gov.

This article contains supporting information online at www.pnas.org/lookup/suppl/doi:10.1073/pnas.1503370112/-/DCSupplemental.

CDX1 function and offer a novel view of the control of phenotypic heterogeneity in tumor cell populations.

Results

MiRNA Profiling of CRC Cell Lines with Low or High CDX1 Expression. To understand the effects of CDX1 on miRNA expression in CRC, we sequenced the small RNA fraction of two pairs of isogenic cell lines with stably modulated CDX1 expression, which had previously been created by Chan et al. (1). The *CDX1* promoter is methylated in HCT116, resulting in low levels of CDX1 expression and an undifferentiated phenotype typified by the formation of dense colonies in vitro and high tumorigenicity in vivo. LS174T, on the other hand, expresses high levels of CDX1 and displays a greater capacity for multilineage differentiation and complex morphology in vitro (1–3, 6). HCT116 was modified to express CDX1 by stable transfection with the constitutively active pRC-CDX1 (HCT116–CDX1) plasmid or empty vector (HCT116-EV). Conversely, endogenous CDX1 expression in LS174T was knocked down by stable transfection of a vector expressing an shRNA targeting CDX1 (LS174T–shCDX1) (Fig. 1*A* and *SI Appendix*, Fig. S1).

The resulting RNA-seq data were aligned to miRBase v.19 and filtered for abundance. Due to the stoichiometric mechanism of miRNA action, by which a miRNA with a greater number of copies in the cell is able to repress a greater number of mRNAs, miRNAs with fewer than 50 normalized mapped reads per million total reads (RPM) were excluded from subsequent analyses as they were deemed unlikely to be physiologically significant (25, 26). Unfiltered data are shown in Dataset S1. The remaining 316 miRNAs were hierarchically clustered according to row-scaled expression, showing a bloc of CDX1-associated expression among ∼1/3 of miRNAs (*SI Appendix*, Fig. S2). Gene set enrichment analysis (GSEA) was conducted using a "gene list" of miRNAs ranked according to differential expression in LS174T (LS174T-EV/LS174T–shCDX1) and a "gene set" of the 100 most differentially expressed miRNAs in HCT116 (HCT116–CDX1/HCT116-EV), which revealed a significant association between differential miRNA expression and CDX1 (normalized enrichment score = 1.33, q = 0.028) (Fig. 1*B*).

To gain an insight as to the direct effects of CDX1 on miRNA expression, we used the Transcription Element Search System (TESS) (27) to interrogate the genomic regions 1 kb upstream of the 10 most up-regulated miRNAs in HCT116 and found a significant enrichment of predicted CDX1 binding sites relative to the regions upstream of 10 randomly selected miRNAs (P = 0.015) (Fig. 1*C*). To assess the differential expression of miRNAs relative to CDX1 status, the fold changes for each miRNA in each pair of isogenic cell lines were calculated as the ratios between HCT116–CDX1(RPM)/HCT116-Vec(RPM) and LS174T-Vec(RPM)/LS174T–siCDX1(RPM) (Fig. 1*D*). Although GSEA had shown a significant enrichment of differentially expressed miRNAs from HCT116 in LS174T, the scatter plot in Fig. 1*D* emphasizes the variation in the magnitude and direction of the differential expression. Indeed, reliance on fold change as a metric of differential expression runs the risk of weighting too highly those miRNAs with low abundance but large fold changes, so for follow-up experiments, we selected as candidate targets of CDX1 those miRNAs with ≥1.5-fold difference between CDX1(+) and CDX1(–) samples in at least one cell line pair, at least 100 RPM in one sample, and predicted upstream CDX1 binding sites. From the results of small RNA-seq of two CDX1-modulated cell-line pairs, we retained eight miRNAs as possible transcriptional targets of CDX1 (Fig. 1*E*).

Analysis of Candidate miRNAs. We chose to validate the results of the small RNA-seq experiment for a group of eight miRNAs with robust levels of expression and large fold differences in relation to CDX1 (Fig. 1*E*) and also with predicted 5′ CDX1 sites and

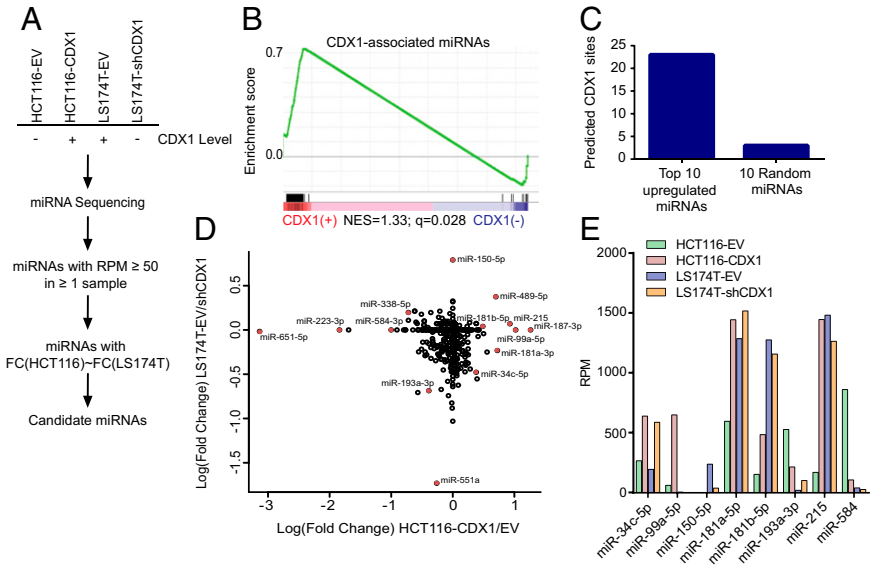

Fig. 1. Small RNA-seq reveals regulation of miRNA expression by CDX1. (*A*) Schema of experimental design for identifying candidate CDX1-regulated miRNAs. FC, fold change. (*B*) GSEA was used to calculate the enrichment of miRNAs up-regulated in HCT116–CDX1 in the set of miRNAs down-regulated by CDX1 knockdown in LS174T. The *Upper* panel shows the running-sum enrichment score. The *Bottom* panel shows the weight of the sum statistic as it varies with the list rank position, from directly associated with CDX1 expression to inversely associated with CDX1 expression. (*C*) The genomic regions 1 kb upstream of the mature sequences of the 10 most up-regulated miRNAs in HCT116–CDX1 were examined for the presence of predicted CDX1 binding sites using TESS. For comparison, we performed the same analysis using 10 random miRNAs. (*D*) The $\log_2$ fold change between CDX1(+) and CDX1(–) samples was calculated for each miRBase-annotated miRNA with RPM ≥ 50 in at least one of the four cell lines subjected to small RNA-seq (i.e., HCT116–CDX1, HCT116-Vec, LS174T–siCDX1, and LS174T-Vec). Each point in the 2D plot represents a different miRNA. Highly expressed miRNAs with large fold changes are labeled and highlighted in red. (*E*) Normalized RNA-seq read counts of candidate CDX1-regulated miRNAs. MiRNAs were selected on the basis of at least 100 reads in one or more cell lines and at least 1.5-fold change in one or more cell line pairs.

a high degree of phylogenetic conservation (*SI Appendix*, Table S1). These criteria were used to select miRNAs that are differentially expressed with respect to CDX1 to an extent likely to be physiologically significant and are also likely to be directly regulated by CDX1 and not by indirect mechanisms. A new batch of total RNA was isolated from the same cell lines used for RNA-seq, and TaqMan probes were used to reverse-transcribe and quantitatively amplify (RT-qPCR) these selected eight miRNAs: miR-34c, miR-99a, miR-150, miR-181a, miR-181b, miR-193a-3p, miR-215, and miR-584. Most of the candidate miRNAs assayed displayed similar fold changes in both RNA-seq and RT-qPCR, with the notable exceptions of miR-193a-3p in HCT116–CDX1/Vec and miR-99a in LS174T-Vec/siCDX1 (*SI Appendix*, Fig. S3). In this and subsequent figures, RT-qPCR results are displayed without error bars or control reference sample data, but with an indication of which differences are statistically significant. See *Materials and Methods* for further discussion of data presentation.

To understand the effects of endogenous variation in CDX1 expression on miRNA expression, we expanded the scope of the RT-qPCR experiment to quantify the expression of these eight candidate miRNAs in a panel of 10 CRC cell lines. The 10 cell lines were grouped into two categories: CDX1 high and CDX1 low (Fig. 2*A*). The CDX1-high group comprised LS180, C80, LIM1863, SW1222, and LS174T, and the CDX1-low group consisted of HCT116, COLO201, SW480, SW620, and C10, all with CDX1 promoter methylation. Candidate miRNA expression in these cell lines was assayed by TaqMan RT-qPCR, and expression levels were calculated relative to the average across all 10 cell lines (Fig. 2*B* and *SI Appendix*, Fig. S4). To determine the association of each candidate miRNA with CDX1 expression, we arranged the expression data from Fig. 2*B* in 2 × 2 contingency tables such that the expression data for a given miRNA were categorized as "high" in a particular cell line if they exceeded the mean expression level [relative quantity (RQ) > 1] and "low" if they were below the mean (RQ < 1). Evaluation of contingency using Fisher's Exact Test (Fig. 2*B* and *SI Appendix*, Table S2) showed miR-215 to be the most, and indeed only, miRNA significantly associated with CDX1 expression in the cell-line panel (P = 0.047). The association of endogenous expression levels of miR-215 and CDX1 was supported by RT-qPCR measurement of miR-215 expression in two additional cell lines (*SI Appendix*, Fig. S5).

Characterization of the miR-215 Primary Transcript. MiR-215 is located on chromosome 1 as a constituent of the miR-194-1–215 cluster. Because clustered miRNAs are typically transcriptionally coregulated (28), we thought it peculiar that miR-194 did not occur in our list of candidate CDX1-regulated miRNAs. To confirm that CDX1 induces miR-215 independently of miR-194, we transiently transfected HCT116 with pRC-CDX1. Expression of CDX1 in the transiently transfected cells was confirmed by Western blot (Fig. 2*C*). After 48 h, we quantitated miR-215 and miR-194 expression relative to EV control. We found miR-215 to be up-regulated by over 2.5-fold, consistent with the results of our small RNA-seq experiment, but the expression levels of miR-194 and an unrelated control miRNA, let-7i, were not affected (Fig. 2*D*).

Although the miR-194–215 primary transcript has previously been implicated in the p53-mediated DNA damage response (29–31), the exact location of the 5′ end of the transcript has thus far eluded efforts to characterize the transcription start site (TSS). The standard method for identifying a TSS, 5′ rapid amplification of cDNA ends (5′RACE) (Fig. 3*A*), is complicated in the case of miRNAs by the short half-life of primary miRNA (pri-miRNA) transcripts. To prolong the half life of pri-miR-194–215, we knocked down expression of the pri-miRNA processing enzyme Drosha in LS174T by transient siRNA transfection. Drosha knockdown was verified by RT-qPCR (Fig. 3*B*). Next, we performed 5′RACE in LS174T after 48 h of siDrosha transfection and successfully isolated and sequenced a band of 148 bp (Fig. 3*C*), which aligned to a genomic position 972 base pairs upstream of the miR-194 stem-loop sequence. The other bands in Fig. 3*C* were also sequenced but did not align to the genome and were likely PCR artifacts. Therefore, we concluded that the 5′ end of the miR-194–215 primary transcript extends 972 bases upstream from the miR-194 sequence and that this is the location of the TSS.

CDX1 Directly Regulates miR-215 Expression. By interpolating the newly discovered location of the miR-194–215 TSS into the CDX1 binding predictions described in Fig. 1*C*, we were able to gain a better picture of the regulatory landscape surrounding the miR-194–215 promoter: the TSS is flanked on the 5′ side by one putative CDX1 site, and four putative CDX1 sites occur at roughly equal intervals in the 972 bp in between the TSS and miR-194 (Fig. 3*D*). To test the dependence of miR-215 promoter activity on CDX1, we created five luciferase reporter constructs

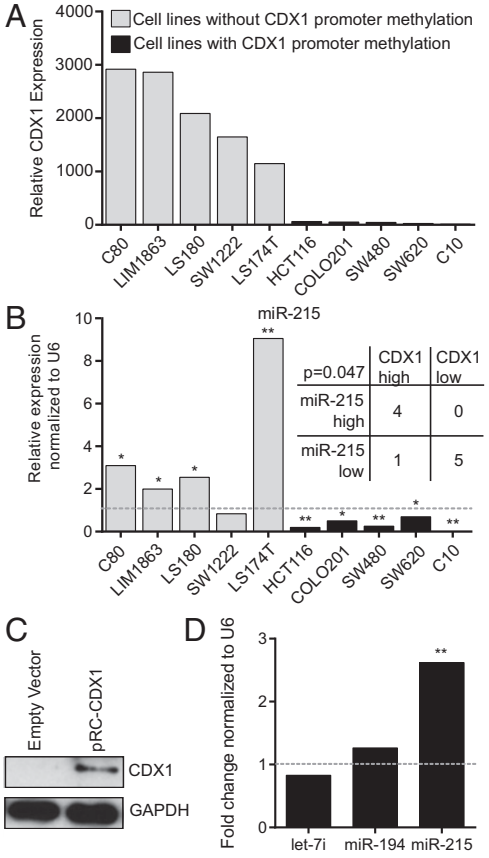

Fig. 2. miR-215 expression is significantly associated with CDX1. (*A*) CDX1 expression in 10 cell lines measured by microarray. (*B*) The expression levels of eight candidate miRNAs shown in Fig. 1*E* were assayed by TaqMan RT-qPCR in five CDX1(+) lines and five CDX1(–) lines, with CDX1 status shown as in *A*. Only miR-215 is shown here; data for the remaining miRNAs are presented in *SI Appendix*, Fig. S4. Ct values were normalized to U6 snRNA, and fold change was calculated relative to the average for a given miRNA across all 10 cell lines. RQ, relative quantity—that is, fold change relative to the average across all cell lines. Cell lines were grouped as CDX1(+) or CDX1(–) according to the data in *A*. Student's t test was performed to determine whether the expression of miR-215 differed significantly from the 10-cell line average for that miRNA. (*C*) Protein lysates were immunoblotted for CDX1 after 48 h of transient transfection of HCT116 with pRC-CDX1 or EV control. (*D*) RNA was isolated from HCT116 transfected as in *C*, and miR-215 and miR-194 expressions were assayed by TaqMan RT-qPCR normalized to U6 snRNA. The unrelated miRNA let-7i is shown as a negative control. Fold-change values are given relative to EV control. *P < 0.05; **P < 0.01.

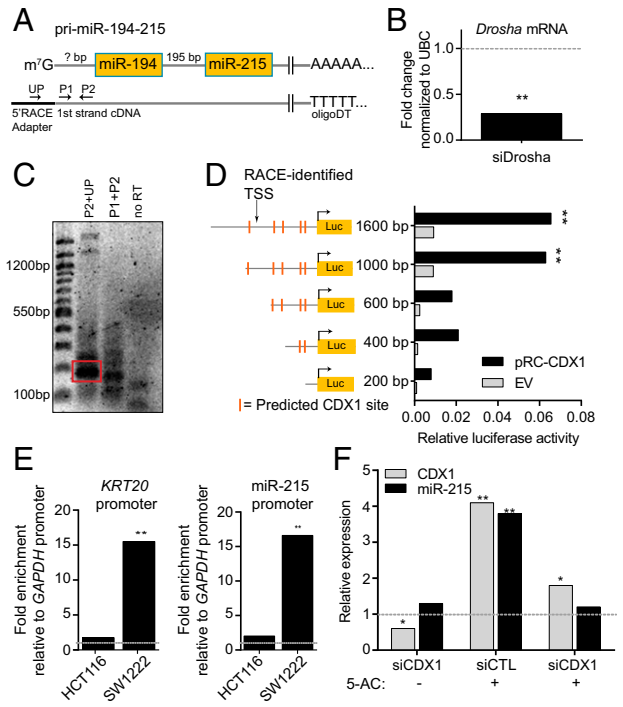

Fig. 3. CDX1 directly regulates miR-215. (*A*) Schema of 5′RACE for the miR-194–215 primary transcript. P1,2, gene-specific primer 1, 2; UP, universal primer specific to RACE adaptor. (*B*) LS174T was transiently transfected with siRNA against Drosha mRNA, and Drosha transcript levels were quantitated by TaqMan RT-qPCR 48 h after transfection. Fold change is shown relative to negative control siRNA (siCTL). (*C*) Total RNA was isolated from LS174T cells following 48 h transfection with siDrosha, and 5′RACE was performed as diagrammed in *A*. The PCR product was electrophoresed on a 3% agarose gel, stained with ethidium bromide, and photographed under trans-UV illumination. The bands were excised and sequenced, and the highlighted band yielded a sequence that aligned to the region upstream from miR-194–215. (*D*) Luciferase reporter constructs were created with the PGL3-firefly backbone containing sequences of the indicated size cloned from the genomic region upstream of miR-215 and were cotransfected into HCT116 along with the *Renilla* luciferase control pRL and either pRC-CDX1 or EV control. Firefly and *Renilla* luminescence measurements were conducted 24 h after transfection. Firefly was normalized to *Renilla* for all samples to yield relative luciferase activity. $n = 3$ independent experiments. (*E*) HCT116 and SW1222 were subjected to ChIP using an anti-CDX1 monoclonal antibody. The enrichment of the miR-215 promoter was determined by qPCR and normalized to the internal control *GAPDH* promoter. Enrichment of the promoter for the independently validated CDX1 target following CDX1 ChIP is shown for comparison. Fold enrichment values are shown relative to input. (*F*) HCT116 cells were treated with 5-AC for 5 d after transfection with either siRNA against CDX1 (siCDX1) or control siRNA (siCTL). Total RNA was isolated, and CDX1 and miR-215 expression levels were assayed by RT-qPCR normalized to GAPDH and U6, respectively. Fold-change values are shown relative to siCTL + mock treatment. $*P < 0.05$; $**P < 0.01$.

containing varying lengths of upstream regulatory sequence and thus varying numbers of putative CDX1 binding sites (Fig. 3*D*). We cotransfected these constructs into HCT116 with either pRC-CDX1 or EV control and measured firefly luciferase activity normalized to a constitutive *Renilla* luciferase cassette after 24 h. The most distal CDX1 binding site, ∼1 kb upstream of the miR-215 sequence, displayed the greatest effect on promoter activity, although the predicted CDX1 sites downstream of the TSS also displayed some capacity for transactivation (Fig. 3*D*). It may be that these sites are responsible to some extent for the selective transactivation by CDX1 of miR-215 as opposed to miR-194. Further targeted mutagenesis experiments would be necessary to evaluate to what extent this is the case.

To confirm direct binding of CDX1 to the endogenous miR-215 promoter, we performed CDX1 ChIP followed by qPCR using primers flanking the core promoter regions of miR-215, as we have defined it, and the well-studied CDX1 target *KRT20* (1). In the CDX1-high cell line SW1222, CDX1 ChIP resulted in ∼15-fold enrichment of both the *KRT20* and miR-215 promoters relative to the *GAPDH* promoter (Fig. 3*E*). Neither the *KRT20* promoter nor the miR-215 promoter was substantially enriched by CDX1 ChIP from the CDX1-low cell line HCT116 (Fig. 3*E*).

As described above, CDX1 expression is controlled by methylation of CpG sites in its promoter region. Therefore, endogenous CDX1 expression may be induced by treatment with the DNA methyltransferase inhibitor 5-aza-2'-deoxycytidine (5-AC). Indeed, treatment of HCT116 with 5-AC for 5 d resulted in a fourfold up-regulation of CDX1 mRNA and a concomitant fourfold increase in miR-215 expression, as determined by RT-qPCR (Fig. 3*F*). Treatment of HCT116 with 5-AC in conjunction with siRNA against CDX1, however, significantly attenuates the up-regulation of both CDX1 and miR-215 (Fig. 3*F*). This result suggests that the increase in miR-215 expression following 5-AC treatment is directly caused by endogenous CDX1.

Identification of Transcriptome-Wide miR-215 Targets. Previous studies of miR-215 have focused on its upstream regulation by p53 and on the effects of its family member, miR-192. To our knowledge, there has been no systematic study of the direct transcriptomic effects of miR-215 expression reported to date. However, before the targets of miR-215 can be identified, the physiological validity of a miR-215 overexpression system must be verified. Using a method that we and others have previously used (21, 32, 33), we quantitated the amount of synthetic miR-215 incorporated into the RNA-induced silencing complex (RISC) following transient transfection of HCT116 with either miR-215 mimic or control (CTL) mimic by immunoprecipitating Ago2 (Fig. 4*A*) and associated RNAs. Our goal was to determine whether the amount of synthetic miR-215 incorporated into RISC after transfection was similar to that of an abundant, endogenously expressed miRNA. We verified the efficacy of Ago2 immunoprecipitation (IP) by Western blot (Fig. 4*A*), which showed that Ago2 protein is specifically precipitated with anti-Ago2 and not IgG (isotype control). Then, RNA was purified from the IPs by phenol:chloroform extraction, and select miRNAs were reverse-transcribed and quantitated by TaqMan RT-qPCR. Fold enrichment was calculated, for each miRNA, relative to control input (i.e., RNA isolated without IP from HCT116 transfected with CTL mimic). The abundant miR-200a was enriched between 40- and 60-fold in Ago2 IP relative to input and was not significantly enriched after IP with IgG. This allowed us to estimate the physiological levels of RISC association. Transfection with CTL or miR-215 mimics did not significantly change the amount of miR-200a enriched in Ago2 IP, indicating that synthetic miRNA mimics do not outcompete endogenous miRNAs for RISC binding. MiR-215 was undetectable in the Ago2 IP from CTL-transfected HCT116 (Fig. 4*B*), which is expected given the very low levels of miR-215 and CDX1 in that cell line (Fig. 2 *A* and *B*). After miR-215 mimic transfection, miR-215 abundance was ∼35-fold greater in Ago2 IP than in CTL input, yet this was substantially lower than the ∼150-fold increase observed in the miR-215 mimic input. These data indicate that simple RT-qPCR measurement of miR-215 in total RNA following miR-215 mimic transfection would overestimate the functional abundance of miR-215 mimic in the cells by nearly fivefold (150/35) and that the actual amount of miR-215 incorporated into RISC is comparable to the physiological levels observed with endogenous miR-200a. Therefore, we concluded that we were unlikely to observe nonspecific effects due to excessive miR-215 levels following mimic transfection. Note that this does not eliminate the possibility of noncanonical effects caused

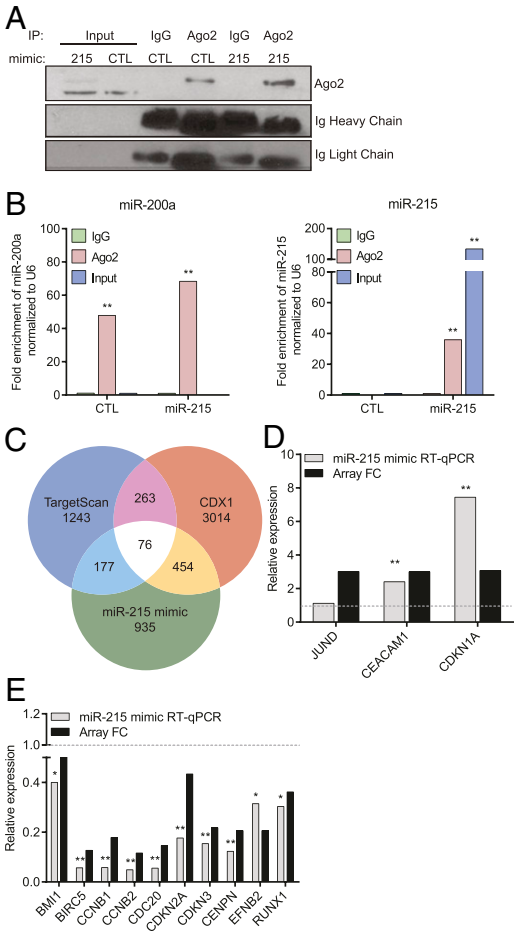

Fig. 4. miR-215 regulates the transcriptome downstream of CDX1. (*A*) Western immunoblot analysis of Ago2 IP. HCT116 was transfected with either miR-215 or CTL mimics. After 48 h, the cells were lysed, and the indicated antibodies were used for IP (isotype control IgG or anti-Ago2). An aliquot of lysate was excluded from IP for analysis as an input control. Ago2 protein was detected in the input lysate and the anti-Ago2 IP, but not the IgG IP. (*B*) HCT116 was transfected with CTL or miR-215 mimics, and IPs were conducted as in *A*. RNA was isolated from the IPs, and miR-200a and miR-215 levels were assayed in each IP condition by RT-qPCR. Fold enrichment values for miR-200a and miR-215 were calculated relative to miR-200a and miR-215 levels, respectively, in CTL-transfected input. (*C*) Venn diagram showing the intersection between the genes significantly down-regulated in the miR-215 microarray, the genes significantly down-regulated in the CDX1 microarray, and the mRNAs predicted to be direct miR-215 targets by TargetScan irrespective of seed conservation. (*D* and *E*) HCT116 was transfected with CTL or miR-215 mimic, RNA was isolated after 24 h, and mRNA expression levels of genes identified as differentially expressed in the microarray were measured using SYBR-Green RT-qPCR. Validation of genes up-regulated in the array is shown in *D*, and down-regulated genes are shown in *E*. Gray bars represent expression levels following independent transfection of CTL or miR-215 mimics; black bar represents fold change miR215/CTL measured in the microarray (Array FC, array fold change). Both the RT-qPCR and the array assays showed similar fold changes for all genes except JUND. $*P < 0.05$; $**P < 0.01$.

by miR-215 mimics acting outside of the RNA-induced silencing pathway.

To identify mRNAs regulated by miR-215, we conducted gene expression profiling following transfection of HCT116 with CTL or miR-215 mimics for 48 h using microarrays. Using an arbitrary fold-change cutoff of 0.6-fold down-regulation relative to CTL and a Bonferroni adjusted *P* value (adj. *P*) cutoff of adj. $P < 0.05$, we obtained a list of 1,642 mRNAs significantly down-regulated by miR-215. It is likely that many of these genes, despite their significant down-regulation in response to miR-215 expression, are repressed by indirect effects; for example, repression of a transcriptional coactivator by miR-215 could indirectly cause down-regulation of many genes. Because we were interested in genes targeted by miR-215 in response to CDX1 expression, we compared the list of genes down-regulated in the miR-215 microarray to a previous microarray study profiling mRNA expression in HCT116-Vec and HCT16–CDX1 (1), reasoning that the intersection of these two microarrays would reflect the most physiologically relevant targets of miR-215 vis-à-vis CDX1. We found 530 genes appearing in both miR-215 and CDX1 down-regulated lists ($P < 10^{-27}$) (Fig. 4*C*). We further compared the list of significantly down-regulated genes in the miR-215 microarray with the complete list of computationally predicted miR-215 targets obtained from the TargetScan algorithm to roughly estimate the extent to which the transcriptomic changes pursuant to miR-215 mimic transfection result from direct targeting of mRNAs by miR-215. We found 253 genes in common between these lists (Fig. 4*C*), which is also a highly significant intersection ($P = 3.7 \times 10^{-14}$). We reasoned that the 76 genes at the intersection of these three sets (Fig. 4*C*) represent the most likely targets of miR-215 downstream of CDX1: those genes that are negatively correlated with both miR-215 and CDX1 and are also computationally predicted direct targets of miR-215.

Differential expression of a manually selected subset of genes from the miR-215 microarray was validated by SYBR-Green RT-qPCR using input RNA from an independent set of miR-215 mimic transfections in HCT116. We chose genes that were significantly differentially expressed in the microarray with large fold changes (Array FC, Array fold change) at both ends of the array's dynamic range, from the strongly up-regulated (Fig. 4*D*) to the strongly down-regulated (Fig. 4*E*). The p53 target *CDKN1A* (p21) and the epithelial cell-surface protein *CEACAM1* were strongly up-regulated in both the array and an orthogonal RT-qPCR assay (Fig. 4*D*). The cell-cycle genes *CDC20*, *CDKN2A*, *CDKN3*, and *CCNB2* were down-regulated in both the array and RT-qPCR (Fig. 4*E*). The negative regulator of apoptosis *BIRC5*, also known as Survivin, was robustly down-regulated, as were the stemness-promoting genes *EFNB2* and *RUNX1* (Fig. 4*E*). The only gene in our sample that was not successfully validated was *JUND* (Fig. 4*D*). The down-regulation of these genes in response to miR-215 overexpression was also validated in the CDX1-low cell line DLD1 and the CDX1-high cell lines LS174T and SW1222 (*SI Appendix*, Fig. S6). Further microarray data are presented in Datasets S2 and S3. Taken together, these data indicate that not only are the transcriptomic effects of miR-215 reproducible across a range of CRC cell lines, but also the high levels of miR-215 in LS174T and SW1222 do not saturate the available targets.

miR-215 Represses the Expression of Stem Cell Genes. MiRNAs canonically repress the expression of their mRNA targets by binding to seed-complementary sequences in the 3′ UTR (15). To verify that miR-215 interacts with its targets in this manner, we cloned the 3′ UTRs from five putative miR-215 target mRNAs selected according to the following criteria: significantly down-regulated in the miR-215 microarray, significantly down-regulated in the CDX1 microarray, contains a miR-215 seed match (i.e., among the 76 genes in the central intersection of Fig. 4*C*), and has been previously reported to be involved in processes related to differentiation and/or CRC biology (*SI Appendix*, Table S3). The five genes chosen on this basis were *BMI1*, *EFNB2*, *EGR1*, *EREG*, and *HOXA10*, and their 3′ UTRs were cloned downstream of the firefly luciferase ORF in the psiCHECK2 vector. These chimeric 3′ UTR luciferase constructs were then cotransfected into HCT116 with either CTL or miR-215 mimics. All five of the tested 3′ UTRs were significantly down-regulated relative to a nontargeting psiCHECK2 EV, yet none were so strongly repressed as the perfectly complementary synthetic target, miR-215–antisense (miR-215 AS) (Fig. 5*A*).

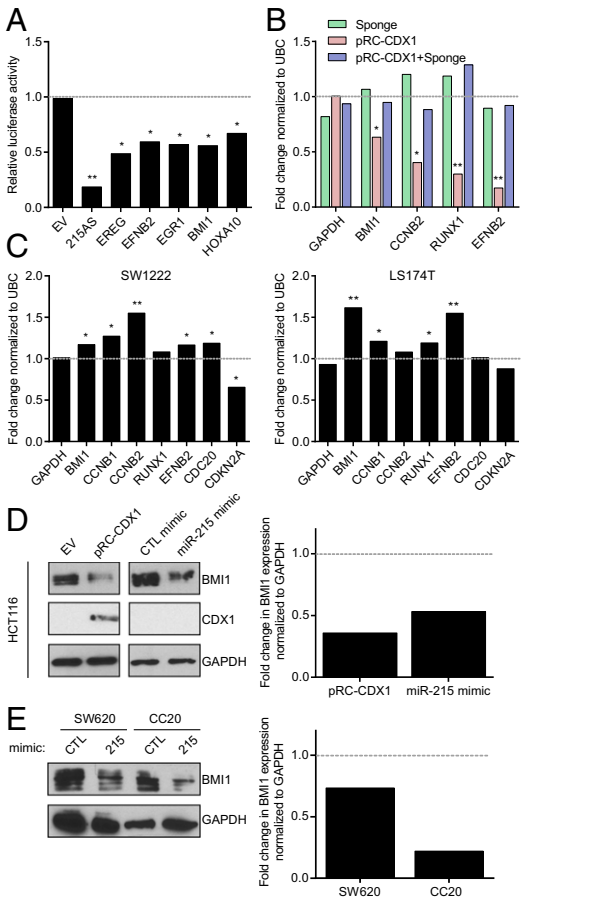

Fig. 5. BMI1 mRNA is directly targeted by miR-215. (*A*) The full-length 3′ UTRs of the indicated genes were cloned into psiCHECK2 downstream of the *Renilla* luciferase ORF. The 3′ UTR constructs were transiently cotransfected into HCT116 for 24 h along with miR-215 or CTL mimics. A repeating array of sequences antisense to mature miR-215 was cloned into psiCHEKC2 as a positive control (215 AS). Cells were lysed and *Renilla* luminescence was normalized to the signal from a constitutively active firefly luciferase cassette in psiCHECK2. Normalized luciferase values are shown relative to CTL mimic. (*B*) HCT116 cells were cotransfected with either miR-215 sponge, pRC-CDX1, a combination of both, or EV for 48 h. RNA was isolated and the mRNA expression levels of five genes down-regulated in both the CDX1 and miR-215 microarrays were assayed by SYBR-Green RT-qPCR. Results are normalized to UBC, and GAPDH is presented as a negative control. Fold change was calculated relative to EV. (*C*) SW1222 and LS174T were transiently transfected with the miR-215 sponge construct or EV for 48 h, total RNA was isolated, and the expression of a subset of miR-215 target genes was assayed by SYBR-Green RT-qPCR. Ct values were normalized to UBC, and the housekeeping gene GAPDH is shown as a control. Fold change is shown relative to EV. (*D*) HCT116 was reverse-transfected for 48 h with either EV, pRC-CDX1, CTL mimic, or miR-215 mimic. Cells were harvested and whole-cell lysate was immunoblotted with antibodies against BMI1 and CDX1, with GAPDH used as a loading control. Intensity of the BMI1 bands was quantitated using densitometry and normalized to GAPDH. (*E*) SW620 and CC20 were reverse-transfected for 48 h with miR-215 or CTL mimics, after which the cells were harvested, lysed, and the lysates were immunoblotted for BMI1 expression with GAPDH as a loading control. Intensity of the BMI1 bands was quantitated using densitometry and normalized to GAPDH. $*P < 0.05$; $**P < 0.01$.

miR-215 Is an Effector of CDX1-Associated Gene Regulation. Having confirmed that miR-215 is a direct transcriptional target of CDX1 that, in turn, mediates the repression of a number of genes, we hypothesized that miR-215 is an important factor in the down-regulation of these genes in response to CDX1 expression. To test this hypothesis, we transfected HCT116 with pRC-CDX1 and a "sponge" construct designed to inhibit miR-215 (*SI Appendix*, Fig. S7 *A* and *B*). The sponge was created as described previously (34) and was validated on the basis of its ability to de-repress a synthetic miR-215 target reporter construct (*SI Appendix*, Fig. S7 *C* and *D*). Transfection of CDX1 alone resulted in significant down-regulation of BMI1, CCNB2, RUNX1, and EFNB2 mRNAs, as we would predict from the results of our microarrays (Fig. 5*B*). Cotransfection with miR-215 sponge, on the other hand, antagonized this down-regulation for all four genes, suggesting that the effect of CDX1 on the expression of these genes depends on miR-215 (Fig. 5*B*). Transfection of the CDX1-high cell lines SW1222 and LS174T with miR-215 sponge had a similar effect, de-repressing a similar set of genes including EFNB2, RUNX1, and BMI1 (Fig. 5*C*).

Previous reports have described an intriguing inverse correlation between CDX1 and BMI1 expression levels, positing CDX1 as a regulator of differentiation that opposes BMI1, a regulator of stemness (6–8). This effect was confirmed by transiently transfecting HCT116 with pRC-CDX1 or EV and measuring BMI1 expression at the protein level (Fig. 5*D*). The effect of CDX1 on BMI1 protein levels is phenocopied by transfection of miR-215 mimic (Fig. 5*D*). We also confirmed the ability of miR-215 to down-regulate BMI1 protein levels in the cell lines SW620 and CC20 (Fig. 5*E*).

miR-215 Is Depleted in the CSC Compartment. Because miR-215 is a direct transcriptional target of CDX1, which promotes differentiation, and targets BMI1 and other important stem cell genes, we reasoned that it may be differentially expressed in differentiated cancer cells compared with cancer stem cells within a given cell line. We used fluorescence-activated cell sorting (FACS) to separate the top 10% of $CD24^+/CD44^+$ cells from the well-differentiated cell lines SW1222 and LS180. Past studies have shown this double-positive subpopulation to be enriched for cancer stem cells with greater clonogenicity, tumorigenicity, and capacity for multilineage differentiation (2). Using TaqMan RT-qPCR, we found miR-215 expression to be ∼10-fold lower in the double-positive subpopulations of these cell lines compared with the unsorted populations (Fig. 6*A*), suggesting that miR-215 is functionally involved in the dynamic process of differentiation and the heterogeneity of phenotypes within a tumor.

Clonogenicity and Differentiation in Vitro Are Repressed by miR-215. Given the above evidence that miR-215 is a functional effector of differentiation downstream of CDX1 in CRC, we attempted to determine the extent to which modulating miR-215 expression could change the clonogenicity and differentiation of cancer cell lines in in vitro experimental systems. First, we transfected five cell lines with low levels of endogenous miR-215 expression—HCT116, DLD1, SW620, CC20, and C10—with CTL or miR-215 mimics. We also included the isogenic p53 knockout variant derived from HCT116, HCT116-$p53^{-/-}$, because previous reports have implicated miR-215 in activation of p53 signaling. After 24 h of transfection, these cells were seeded in the 3D cell culture medium matrigel and allowed to grow for 2 wk. We noticed a significant decrease in the number of colonies initiated by the miR-215–transfected cells compared with the CTL transfectants in all cell lines except for CC20 (Fig. 6*B*). However, in CC20, there was a readily observable difference in morphology between the miR-215 and CTL transfectants, with the miR-215–transfected cells adopting a far more widespread network morphology than the CTL cells, which formed mostly round, circumscribed colonies (Fig. 6 *C* and *D* and *SI Appendix*, Fig. S8). Our studies of the 3D morphologies of a wide panel of CRC cell lines have indicated that the network morphology is a characteristic differentiated form adopted by CC20 (35), and the preference for this morphology following miR-215 transfection is consistent with the idea that it promotes a more differentiated state in the cell line. We further observed that CDX1 expression promotes a complex, lobular morphology in matrigel. This effect is attenuated by antagonization of miR-215, which indicates that

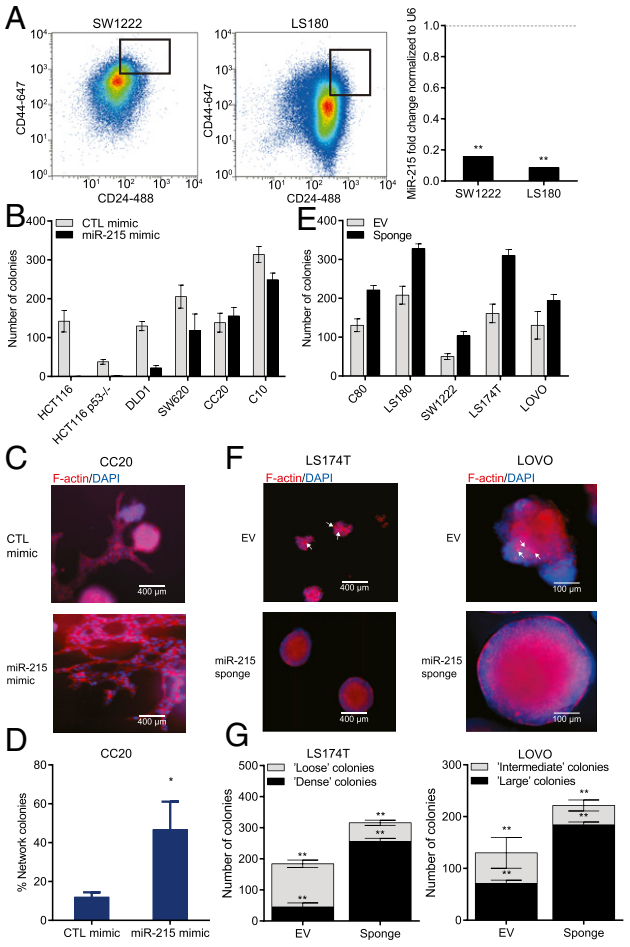

Fig. 6. miR-215 inhibits stemness in vitro. (*A*) LS180 and SW1222 cell lines were costained with CD24–AlexaFluor-488 and CD44–AlexaFluor-647 antibody conjugates. The top 10% of CD24/CD44 double-positive cells was collected from each cell line by FACS. RNA was isolated from the sorted cells, and miR-215 expression was quantitated by TaqMan RT-qPCR and normalized to U6. Fold change was calculated relative to U6-normalized miR-215 expression in unsorted cells. (*B*) The CDX1/miR-215–low cell lines HCT116, HCT116-p53$^{-/-}$, DLD1, SW620, CC20, and C10 were reverse-transfected with CTL or miR-215 mimic for 24 h and then seeded in matrigel diluted 1:1 with DMEM. The colonies were grown for 2 wk and counted under a light microscope. (*C*) CC20 3D morphology in matrigel following miR-215 transfection was observed by fixing the matrigel-grown colonies and staining filamentous actin (F-actin) with phalloidin:TRITC (red). Nuclei were counterstained with DAPI (blue). (*D*) Some CC20 colonies formed continuous sheets or "networks" extending laterally across the surface of the well. The area of each well covered by networks was measured with a light microscope-affixed graticule and plotted as a percentage of the total surface area. (*E*) The CDX1/miR-215–high cell lines C80, LS180, SW1222, LS174T, and LOVO were transfected with miR-215 sponge or EV for 24 h; seeded in matrigel; and counted after 2 wk as in *B*. (*F*) 3D morphology changes following miR-215 knockdown in LS174T and LOVO were observed by F-actin and DAPI staining as in *C*. Several F-actin foci are indicated with white arrows. (*G*) Enumeration of morphological changes shown in *F*, with miR-215 sponge transfection resulting in a clear shift toward a dense colony shape. $*P < 0.05$; $**P < 0.01$.

although miR-215 may not be sufficient to induce morphological changes in all cell lines, it is necessary for the effects downstream of CDX1 (*SI Appendix*, Fig. S9). We also considered that the effect of miR-215 on colony formation could be partly due to growth arrest and inhibition of proliferation, yet any effect on cell proliferation on plastic following miR-215 mimic transfection was far more subtle than the effects on colony growth in matrigel (*SI Appendix*, Fig. S10). This further suggested that the effects of miR-215 are primarily on differentiation of the stem cell compartment rather than growth arrest of the proliferative compartment.

We also examined the effects of knocking down endogenous miR-215 in five well-differentiated cell lines: C80, LS180, LS174T, SW1222, and LOVO. We found that the clonogenicity of four out of these five cell lines could be significantly increased by transfection with miR-215 sponge, as determined by an increased rate of colony formation in matrigel relative to transfection with EV (Fig. 6*E*). The cell lines LS174T and LOVO, in addition to forming more total colonies after miR-215 knockdown, also displayed a marked shift away from their typical morphologies and toward a larger, denser, regularly spherical colony shape. EV-transfected LS174T colonies were small and irregularly shaped with punctate filamentous actin (F-actin) foci, indicating polarization and a degree of functional differentiation (3). Transfection with miR-215 sponge caused an increase in the proportion of larger, round, circumscribed colonies without F-actin foci (Fig. 6*F* and *SI Appendix*, Fig. S11). Similarly, EV-transfected LOVO colonies had irregular borders with scattered areas of F-actin polarization, which were mostly absent from large, round colonies following miR-215 sponge transfection (Fig. 6*F* and *SI Appendix*, Fig. S12). These changes were quantitated, and for both cell lines the number of dense colonies increased by ∼100% following miR-215 knockdown compared with EV transfection, whereas the number of irregularly shaped (loose or intermediate, respectively) colonies did not change significantly (Fig. 6*G*). These results further support a role for miR-215 in promoting a differentiated phenotype in CRC.

Discussion

The work presented in this paper implicates miR-215 in the transcriptional network regulated by CDX1. By profiling miRNA expression in cell lines with modulated CDX1 expression, we identified several miRNAs that were either up- or down-regulated in response to CDX1. A key method used in the identification of miR-215 as an important target of CDX1 was profiling candidate miRNA expression in 10 colorectal cell lines with varying CDX1 expression. We were able to detect a robust relationship that is maintained across cell lines with varying mutation and gene expression landscapes. We used several standard biochemical and molecular biology techniques to verify the transactivation of miR-215 by CDX1. ChIP, in particular, demonstrated that CDX1 binds as strongly to the miR-215 promoter as to a previously characterized, protein-coding CDX1 target gene, *KRT20* (1). This result is consistent with our hypothesis that miR-215 is equally important as a mediator of the effects of CDX1 compared with protein coding genes.

Although previous studies of miR-215 have grouped it together with the related cluster of miR-192–194-2 (29–31), our data did not suggest that CDX1 regulates the transcription of miR-194-1, miR-192, or miR-194-2. This observation suggests previously undetected diversity of function within this miRNA family. Furthermore, this study is the first, to our knowledge, to validate the direct targets of miR-215 from microarray data. Earlier studies on miR-215 have, instead, focused on mRNAs targeted by miR-192. Although miR-215 and miR-192 share the same seed sequence, miRNA:mRNA complementarity outside the seed sequence may also play a role in target specificity (25). In fact, we report a biologically important target of miR-215 with only a partial seed match, namely BMI1.

Previous studies on the effects of CDX1, based on microarray gene expression profiles from 110 CRC cell lines, have shown a robust negative association between CDX1 and BMI1 expression (2, 6). This negative correlation is thought to be tied to the role of CDX1 as a regulator of differentiation in the colon and to the role of *BMI1* as a marker and a regulator of a crypt-base stem cell population (7, 8, 36). In cancers with methylated *CDX1*, BMI1

expression is high, which corresponds to incomplete differentiation, a high proportion of cancer stem cells, and a more aggressive growth profile. Conversely, high CDX1 expression correlates with low BMI1 expression, a well-differentiated tumor, and a less aggressive phenotype (2, 6, 37). Overexpression of BMI1 has been shown to promote clonogenicity in CRC cell lines and inhibit the formation of differentiated colony morphologies in vitro (35), which clearly mirrors the effects of miR-215. The mechanism underlying the correlation between CDX1 and BMI1 expression has proven elusive, as CDX1 is, canonically, a transcriptional activator (38), so a direct, negative interaction between CDX1 and BMI1 would seem counterintuitive. We therefore propose that miR-215 acts as part of a CDX1-mediated differentiation switch. In the case of the normal intestinal crypt, as cells migrate upwards along the crypt through the transit amplifying zone, CDX1 expression is activated, which represses BMI1 through miR-215. In the case of a tumor, CDX1 and miR-215 expression likely underlie the phenotypic heterogeneity in tumors consisting of cancer stem cell subpopulations that give rise to differentiated tumor cells. This argument is further supported by the lack of miR-215 expression in the cancer stem cell-enriched fractions of differentiated cell lines. Significantly, aberrant miR-215 expression is also coincident with CDX1 activation in Barrett's esophagus (13, 39), suggesting that this axis is important in intestinal metaplasia (40).

Previous studies on the roles of miRNAs in regulating differentiation have indicated that they act as switches—for example, miR-489 regulating the transition from muscle stem cell quiescence to proliferation (41) or miR-34a regulating cell-fate decisions in the intestinal crypt by repressing Notch signaling (42). In cancer cell lines, we have observed that miR-215 expression can both inhibit the clonogenicity and promote the adoption of differentiated morphologies. Indeed, a recent study by Kreso et al. demonstrated strikingly similar effects of small-molecule inhibition and siRNA knockdown of BMI1 in CRCs in vitro (43). Further studies of the role of miR-215 in multilineage differentiation in the normal gut and in CRC will be necessary to understand more precisely the stage at which miR-215 expression is involved in promoting differentiation in vivo.

The identification of miR-215 as an effector of CDX1 and a repressor of BMI1 not only suggests future avenues for the study of differentiation in the normal gut, but it also points to a physiological pathway that may be therapeutically reconstituted to treat CRC. Clinical use of miRNAs in cancer treatment has advanced significantly in recent years (44, 45). We therefore propose that miR-215 has significant promise as a therapeutic effector of anticancer molecular pathways, based both on previous reports of its involvement in p53 signaling and the present study of its inhibition of cancer stem cells.

Materials and Methods

Cell Culture. All cell lines were obtained from cryogenic storage in the Cancer and Immunogenetics Laboratory. The cell lines C80, HCT116–CDX1, HCT116-EV, LS174T–siCDX1, and LS174T-EV were created in-house (1). The SW1222 and HCT116-p53$^{-/-}$ cell lines were generously provided by Meenhard Herlyn (Wistar Institute, Philadelphia, PA) and Bert Vogelstein (Johns Hopkins, Baltimore, MD), respectively. The remaining cell lines were originally purchased from ATCC or The European Collection of Cell Cultures. All cell lines were maintained in Dulbecco's modified Eagle medium (DMEM, Gibco) containing 10% (vol/vol) FBS at 37 °C and 5% CO_2.

3D Cell Culture. Culture of colorectal cell lines in matrigel was performed as previously described (1–3). Briefly, cells cultured on plastic were harvested with 1% Trypsin-EDTA (Gibco) and counted using a Nexcelcom AutoT4 Cellometer automated cell counter. Cells were then diluted with DMEM to a concentration of 2×10^4/mL and added in a 1:1 ratio to 10 mg/mL matrigel (BD Corning). We plated 50 μL of the cell:matrigel dilution per well of a 96-well plate and incubated it for 30 min at 37 °C. After the gel had solidified, the cells were overlaid with 150 μL DMEM and grown in standard conditions, with medium changed every 48 h. After 2 wk, the colonies were fixed in 4% formaldehyde for 15 min, and then the cells were permeableized with a 1% Triton-X100 (Thermo Fisher) detergent solution. The colonies were washed three times with PBS, and 150 μL of a 1:1,000 dilution of phalloidin-TRITC conjugate (Life Technologies) in PBS was added to the cells. We added 10 μL of DAPI to stain the nuclei. Cells were then incubated overnight at 4 °C in the dark. After another wash with PBS, the cells were imaged on an Axio Vert inverted fluorescent microscope (Zeiss).

Flow Cytometry. FACS was used to sort cells by flow cytometry on the basis of CD24/CD44 coexpression. This method was performed as described previously (2). In short, cells were trypsinized, washed, and resuspended at a density of 1×10^7 cells/mL in a solution containing a 1:20,000 dilution of AlexaFluor-488 conjugated anti-CD44 and AlexaFluor-647 conjugated anti-CD44 (Invitrogen). Cells were sorted with a MoFlo cell sorter (Beckman Coulter).

Immunoblotting. Cultured cells were lysed using radioimmunoprecipitation buffer (RIPA buffer, Millipore) containing a protease inhibitor cocktail (Roche). Total protein concentration of whole-cell lysates was determined using the Thermo BCA kit (Thermo Fisher). We boiled 10 μg of protein in SDS sample buffer (National Diagnostics) and separated it using SDS/PAGE. After semidry transfer to a PVDF membrane, proteins were probed using the following antibodies and dilutions: Ago2 (gift of Zissimos Mourelatos, University of Pennsylvania, Philadelphia) at 1:5,000 dilution, BMI1 (Clone 2830, Cell Signaling) at 1:10,000 dilution, CDX1 (in-house) (1) at 1:2,000, and GAPDH (Clone 14C10, Cell Signaling) at 1:10,000.

IP. CDX1 ChIP was carried out using the Active Motif ChIP kit. The CDX1 monoclonal antibody was produced in-house at the Cancer and Immunogenetics Lab (1). HCT116 cells were grown in 15-cm dishes to 80% confluence, crosslinked in 1% formaldehyde, lysed, and sonicated to shear the chromatin. The sheared chromatin was then incubated overnight at 4° with antibody-paramagnetic bead complexes containing either IgG or anti-CDX1. IP material was washed and incubated overnight at 65° to reverse the crosslinks. Immunoprecipitated DNA was then column purified (Qiagen). qPCR was performed to quantitate ChIP enrichment using primers flanking the miR-215 and *KRT20* promoter regions. AGO2 IP was performed as described previously (21, 33, 46). Briefly, HCT116 cells were transfected with miR-215 or CTL mimics as described above. The transfectants were then lysed using RIPA buffer (Millipore) and treated with a protease inhibitor mixture (Roche) and RNaseOUT (Invitrogen). The lysate was incubated with IgG or anti-Ago2 and precipitated with protein-G Sepharose Dynabeads (Invitrogen) beads. RNA was isolated by phenol:chloroform extraction followed by ethanol precipitation. MiRNA enrichment was subsequently assayed by TaqMan RT-qPCR.

Luciferase Reporter Assays. Luciferase reporter assays were carried out using the Dual-Luciferase Reporter Assay System kit (Promega). pGL3 and pRL were used for promoter luciferase, and psiCHECK2 was used for 3′ UTR luciferase. For testing the miR-215 promoter, HCT116 was transiently transfected with three plasmids: the constitutively active *Renilla* luciferase-expressing vector pRL to control for transfection efficiency; one of the 1.0-, 0.6-, 0.4-, or 0.2-kb miR-215 promoter constructs in the pGL3 firefly luciferase-expressing vector; and the constitutively active CDX1-expressing vector pRC/CMV–CDX1. For 3′ UTR luciferase assays to identify miR-215 targets, the full-length 3′ UTR of a gene of interest was cloned downstream of the *Renilla* ORF in the psiCHECK2 vector. Chimeric *Renilla* luciferase–human 3′ UTR constructs were transiently transfected into HCT116. PsiCHECK2 also encodes a constitutive firefly luciferase gene, which is used for normalization. In both types of experiments, luciferase activity was measured after 24 h per the manufacturer's instructions. All primer sequences used for cloning are given in *SI Appendix*, Table S4.

Small RNA Sequencing. Total RNA was size fractionated by denaturing PAGE, from which RNAs 18–30 nt in length were purified. The small RNA fraction was ligated to Illumina sequencing adapters and used as a template for the creation of a cDNA library. Libraries were sequenced on an Illumina Genome Analyzer II platform (Illumina). Illumina small RNA sequencing adapters were removed from the sequence data before alignment to the Hg19 reference genome using Burrows-Wheeler Aligner. Expression levels were estimated from the aligned data by counting the number of read-tags overlapping the genomic location of mature miRNA loci, separately for matches to the positive and negative strands. Read counts were normalized by dividing counts by the average of the read count for mature miRNA in the second and third quartile of strand-selected reads. Small RNA-seq data are given in Dataset S1.

RNA Isolation, RT-qPCR, and miRNA Analysis. MiRNAs were purified from CRC cell lines using the miRNEasy kit (Qiagen). Total RNA for mRNA quantitation was prepared using TRIzol reagent (Invitrogen). RNA quality was determined by analysis with a NanoDrop spectrophotometer (Thermo Fisher). For miRNA RT-qPCR, predesigned TaqMan primers and probes were ordered from Life Technologies. Total RNA was reverse-transcribed using iScript cDNA Synthesis Master Mix (Bio-Rad) for reverse transcription. qPCR was then performed using SYBR-Green chemistry (Roche). All primer sequences used for SYBR-Green RT-qPCR are given in *SI Appendix*, Table S5. RT-qPCR calculations and data presentation are briefly discussed in *Statistical Methods*.

Statistical Methods. All error bars are given as ±SD of the mean for three biological replicates, unless otherwise noted. *P* values for RT-qPCR data, luciferase data, and colony formation data were calculated using two-tailed Student's *t* test assuming unequal variance. Error bars are not shown for RT-qPCR data, as the exponential transformation involved in calculating fold change does not preserve the variance in the primary data. Statistically significant differences are, instead, indicated by asterisks denoting *P* values obtained by *t* tests of ΔC_T values. Fold-change values for RT-qPCR are calculated using the $\Delta\Delta C_T$ method relative to a control sample. As the fold change for the control is always defined as 1, we chose not to plot control data points in RT-qPCR figures, instead showing a dotted line at 1. We evaluated 2×2 contingency tables using Fisher's exact test. Gene set enrichment analysis was performed as described previously using the GSEA Java application (47, 48). CDX1 binding sites were interrogated using the TESS web application (now defunct; source code available at www.cbil.upenn.edu/tess) (27). Intersection of microarray gene sets was modeled on sampling without replacement from the hypergeometric probability distribution using the phyper function in the R programming environment.

Transfections. Luciferase reporter plasmids were transfected into HCT116 cells seeded in 12-well plates using Lipofectamine 2000 (Invitrogen) per the manufacturer's suggestions. MiR-215 sponge was constructed as described previously (34) and as shown in *SI Appendix*, Fig. S7. Sponge constructs were forward-transfected in six-well plates using Lipofectamine 2000 with 1 μg plasmid per well. The CDX1 expression vector pRC-CDX1 was previously created in-house (1). PRC-CDX1 was forward-transfected in six-well plates using Lipofectamine 2000 with 500 ng per well. MiRNA mimics were purchased from Dharmacon and reverse-transfected in six-well plates at a final concentration of 20 nM using Lipofectamine RNAiMax (Invitrogen) per the manufacturer's instructions. SiRNAs were purchased from Qiagen and reverse-transfected in six-well plates at a final concentration of 50 nM using Lipofectamine RNAiMax.

ACKNOWLEDGMENTS. We thank Jennifer Wilding for helpful discussions and Kevin Clark and Craig Waugh for their FACS expertise. This research was supported, in part, by the Intramural Research Program of the National Institutes of Health, National Cancer Institute. M.F.J. was supported by a Marshall Scholarship and a National Institutes of Health Ox-Cam Fellowship.

1. Chan CWM, et al. (2009) Gastrointestinal differentiation marker Cytokeratin 20 is regulated by homeobox gene CDX1. *Proc Natl Acad Sci USA* 106(6):1936–1941.
2. Yeung TM, Gandhi SC, Wilding JL, Muschel R, Bodmer WF (2010) Cancer stem cells from colorectal cancer-derived cell lines. *Proc Natl Acad Sci USA* 107(8):3722–3727.
3. Ashley N, Yeung TM, Bodmer WF (2013) Stem cell differentiation and lumen formation in colorectal cancer cell lines and primary tumors. *Cancer Res* 73(18):5798–5809.
4. Wong NA, et al. (2004) Loss of CDX1 expression in colorectal carcinoma: Promoter methylation, mutation, and loss of heterozygosity analyses of 37 cell lines. *Proc Natl Acad Sci USA* 101(2):574–579.
5. Pilozzi E, Onelli MR, Ziparo V, Mercantini P, Ruco L (2004) CDX1 expression is reduced in colorectal carcinoma and is associated with promoter hypermethylation. *J Pathol* 204(3):289–295.
6. Yeung TM, Gandhi SC, Bodmer WF (2011) Hypoxia and lineage specification of cell line-derived colorectal cancer stem cells. *Proc Natl Acad Sci USA* 108(11):4382–4387.
7. Yan KS, et al. (2012) The intestinal stem cell markers Bmi1 and Lgr5 identify two functionally distinct populations. *Proc Natl Acad Sci USA* 109(2):466–471.
8. Tian H, et al. (2011) A reserve stem cell population in small intestine renders Lgr5-positive cells dispensable. *Nature* 478(7368):255–259.
9. Arango D, et al. (2012) Villin expression is frequently lost in poorly differentiated colon cancer. *Am J Pathol* 180(4):1509–1521.
10. Staloch LJ, Divine JK, Witten JT, Simon TC (2005) C/EBP and Cdx family factors regulate liver fatty acid binding protein transgene expression in the small intestinal epithelium. *Biochim Biophys Acta* 1731(3):168–178.
11. Mutoh H, et al. (2004) Cdx1 induced intestinal metaplasia in the transgenic mouse stomach: Comparative study with Cdx2 transgenic mice. *Gut* 53(10):1416–1423.
12. Fujii Y, et al. (2012) CDX1 confers intestinal phenotype on gastric epithelial cells via induction of stemness-associated reprogramming factors SALL4 and KLF5. *Proc Natl Acad Sci USA* 109(50):20584–20589.
13. Wong NA, et al. (2005) CDX1 is an important molecular mediator of Barrett's metaplasia. *Proc Natl Acad Sci USA* 102(21):7565–7570.
14. Hermeking H (2012) MicroRNAs in the p53 network: Micromanagement of tumour suppression. *Nat Rev Cancer* 12(9):613–626.
15. Kim VN, Han J, Siomi MC (2009) Biogenesis of small RNAs in animals. *Nat Rev Mol Cell Biol* 10:126–139.
16. Lu J, et al. (2005) MicroRNA expression profiles classify human cancers. *Nature* 435(7043):834–838.
17. Dvinge H, et al. (2013) The shaping and functional consequences of the microRNA landscape in breast cancer. *Nature* 497(7449):378–382.
18. Kumar MS, et al. (2009) Dicer1 functions as a haploinsufficient tumor suppressor. *Genes Dev* 23(23):2700–2704.
19. Calin GA, et al. (2004) Human microRNA genes are frequently located at fragile sites and genomic regions involved in cancers. *Proc Natl Acad Sci USA* 101(9):2999–3004.
20. Jones M, Lal A (2012) MicroRNAs, wild-type and mutant p53: More questions than answers. *RNA Biol* 9(6):781–791.
21. Subramanian M, et al. (2014) A mutant p53/let-7i-axis-regulated gene network drives cell migration, invasion and metastasis. *Oncogene*.
22. Okada N, et al. (2014) A positive feedback between p53 and miR-34 miRNAs mediates tumor suppression. *Genes Dev* 28(5):438–450.
23. Chang T-C, et al. (2007) Transactivation of miR-34a by p53 broadly influences gene expression and promotes apoptosis. *Mol Cell* 26(5):745–752.
24. Masciarelli S, et al. (2014) Gain-of-function mutant p53 downregulates miR-223 contributing to chemoresistance of cultured tumor cells. *Oncogene* 33(12):1601–1608.
25. Ameres SL, Zamore PD (2013) Diversifying microRNA sequence and function. *Nat Rev Mol Cell Biol* 14(8):475–488.
26. Creighton CJ, Reid JG, Gunaratne PH (2009) Expression profiling of microRNAs by deep sequencing. *Brief Bioinform* 10(5):490–497.
27. Schug J (2008) Using TESS to predict transcription factor binding sites in DNA sequence. *Curr Protoc Bioinformatics* Chapter 2:Unit 2.6.
28. He L, et al. (2005) A microRNA polycistron as a potential human oncogene. *Nature* 435(7043):828–833.
29. Braun CJ, et al. (2008) p53-responsive micrornas 192 and 215 are capable of inducing cell cycle arrest. *Cancer Res* 68(24):10094–10104.
30. Georges SA, et al. (2008) Coordinated regulation of cell cycle transcripts by p53-inducible microRNAs, miR-192 and miR-215. *Cancer Res* 68(24):10105–10112.
31. Pichiorri F, et al. (2010) Downregulation of p53-inducible microRNAs 192, 194, and 215 impairs the p53/MDM2 autoregulatory loop in multiple myeloma development. *Cancer Cell* 18(4):367–381.
32. Thomson DW, Bracken CP, Szubert JM, Goodall GJ (2013) On measuring miRNAs after transient transfection of mimics or antisense inhibitors. *PLoS ONE* 8(1):e55214.
33. Li XL, et al. (2014) A p21-ZEB1 complex inhibits epithelial-mesenchymal transition through the microRNA 183-96-182 cluster. *Mol Cell Biol* 34(3):533–550.
34. Kluiver J, et al. (2012) Rapid generation of microRNA sponges for microRNA inhibition. *PLoS ONE* 7(1):e29275.
35. Ghandi S (2010) Regulation of stemness and differentiation in colorectal cancer. PhD dissertation (University of Oxford, Oxford, UK). Available at ora.ox.ac.uk/objects/uuid:a32fd55a-4b1e-4a15-9f79-9fdbd986774a.
36. Sangiorgi E, Capecchi MR (2008) Bmi1 is expressed in vivo in intestinal stem cells. *Nat Genet* 40(7):915–920.
37. Ashley N, Jones M, Ouaret D, Wilding J, Bodmer WF (2014) Rapidly derived colorectal cancer cultures recapitulate parental cancer characteristics and enable personalized therapeutic assays. *J Pathol* 234(1):34–45.
38. Gautier-Stein A, et al. (2003) Differential regulation of the glucose-6-phosphatase TATA box by intestine-specific homeodomain proteins CDX1 and CDX2. *Nucleic Acids Res* 31(18):5238–5246.
39. Wijnhoven BPL, et al.; South Australian Oesophageal Research Group (2010) MicroRNA profiling of Barrett's oesophagus and oesophageal adenocarcinoma. *Br J Surg* 97(6):853–861.
40. Lavery DL, et al. (2014) The stem cell organisation, and the proliferative and gene expression profile of Barrett's epithelium, replicates pyloric-type gastric glands. *Gut* 63(12):1854–1863.
41. Cheung TH, et al. (2012) Maintenance of muscle stem-cell quiescence by microRNA-489. *Nature* 482(7386):524–528.
42. Bu P, et al. (2013) A microRNA miR-34a-regulated bimodal switch targets Notch in colon cancer stem cells. *Cell Stem Cell* 12(5):602–615.
43. Kreso A, et al. (2014) Self-renewal as a therapeutic target in human colorectal cancer. *Nat Med* 20(1):29–36.
44. Kasinski AL, Slack FJ (2011) Epigenetics and genetics. MicroRNAs en route to the clinic: Progress in validating and targeting microRNAs for cancer therapy. *Nat Rev Cancer* 11(12):849–864.
45. Broderick JA, Zamore PD (2011) MicroRNA therapeutics. *Gene Ther* 18(12):1104–1110.
46. Lal A, et al. (2011) Capture of microRNA-bound mRNAs identifies the tumor suppressor miR-34a as a regulator of growth factor signaling. *PloS Genet* 7(11):e1002363.
47. Subramanian A, et al. (2005) Gene set enrichment analysis: A knowledge-based approach for interpreting genome-wide expression profiles. *Proc Natl Acad Sci USA* 102(43):15545–15550.
48. Mootha VK, et al. (2003) PGC-1alpha-responsive genes involved in oxidative phosphorylation are coordinately downregulated in human diabetes. *Nat Genet* 34(3):267–273.